Proteome changes induced by a short, non-cytotoxic exposure to the mycoestrogen zearalenone in the pig intestine

Laura Soler, Stella Alexandre, Seva Juan, Pallarés Francisco José, Lahjouji Tarek, Burlet-Schiltz Odile, Isabelle P. Oswald

Title. Proteome changes induced by a short, non-cytotoxic exposure to the mycoestrogen zearalenone in the pig intestine

Authors: Soler Laura[a*], Stella Alexandre[b], Seva Juan[c], Pallarés Francisco José[c], Lahjouji Tarek[a], Burlet-Schiltz Odile[b], Oswald Isabelle P. [a,]

[a]Toxalim (Research Centre in Food Toxicology), Université de Toulouse, INRAE, ENVT, INP-Purpan, UPS, Toulouse, France

[b]Toulouse Proteomics Infrastructure, Institut de Pharmacologie et Biologie Structurale (IPBS), Université de Toulouse, CNRS, UPS, Toulouse, France

[c]Department of Anatomy and Comparative Pathology, Faculty of Veterinary Medicine, University of Murcia, Mare Nostrum Excellence Campus, Murcia, Spain.

* Correspondence to:

Laura Soler

Toxalim (Research Centre in Food Toxicology), Université de Toulouse, INRAE, ENVT, INP-Purpan, UPS, Toulouse, France

Tel + 33 5 82 06 63 66

e-mail : laura.soler-vasco@inrae.fr

Abstract

Intestinal epithelial homeostasis is regulated by a complex network of signaling pathways. Among them is estrogen signaling, important for the proliferation and differentiation of epithelial cells, immune signaling and metabolism. The mycotoxin zearalenone (ZEN) is an estrogen disruptor naturally found in food and feed. The exposure of the intestine to ZEN has toxic effects including alteration of the immune status and is possibly implicated in carcinogenesis, but the molecular mechanisms linked with these effects are not clear. Our objective was to explore the proteome changes induced by a short, non-cytotoxic exposure to ZEN in the intestine using pig jejunal explants. Our results indicated that ZEN promotes little proteome changes, but significantly related with an induction of ERα signaling and a consequent disruption of highly interrelated signaling cascades, such as NF-κB, ERK1/2, CDX2 and HIF1α. The toxicity of ZEN leads also to an altered immune status characterized by the activation of the chemokine CXCR4/SDF-1 axis and an accumulation of MHC-I proteins. Our results connect the estrogen disrupting activity of ZEN with its intestinal toxic effect, associating the exposure to ZEN with cell-signaling disorders similar to those involved in the onset and progression of diseases such as cancer and chronic inflammatory disorders.

Significance

The proteomics results presented in our study indicate that the endocrine disruptor activity of ZEN is able to regulate a cascade of highly inter-connected signaling events essential for the small intestinal crypt-villus cycle and immune status. These molecular mechanisms are also implicated in the onset and progress of intestinal immune disorders and cancer indicating that exposure to ZEN could play an important role in intestinal pathogenesis.

Keywords

mycotoxins; zearalenone; intestine; pig; estrogen receptors; proteomics

Highlights

-Zearalenone (ZEN) is an estrogenic toxic food contaminant produced by certain molds.

-A short, non-cytotoxic exposure to ZEN induced little changes in the intestinal proteome, but they were significantly pointing at a disruption of estrogen signaling.

-The estrogenic response activated by ZEN induced changes in the abundance of proteins that mediate important intestinal functions related with epithelial homeostasis and immune status.

-ZEN could contribute to the pathogenesis of important intestinal diseases, such as inflammatory bowel diseases and cancer.

1. Introduction

Several fungal species that grow on crops are able to synthesize secondary toxic metabolites (mycotoxins) under certain environmental conditions. These mycotoxins constitute natural food contaminants. Zearalenone (ZEN) is a mycotoxin produced by several *Fusarium* species and is frequently found mostly in cereals in temperate regions of the world [1,2]. Because of the structural similarity between ZEN and the hormone 17-β-estradiol (E2), ZEN is able to bind estrogen receptors (ERs), exerting an endocrine disruption effect [3]. The toxic effect of ZEN in the reproductive system is well known, and include infertility, hormonal dysfunctions and hyperplasia [4]. ZEN is also toxic to other organs, especially those that are estrogen responding, such as the liver [5–7], immune cells [8–11] and the intestine [12–14]. ZEN is a full agonist of estrogen receptor α (ERα) and a mixed agonist/antagonist of estrogen receptor β (ERβ) [15]. The estrogenic stimulation by ZEN, like that of E2, is predominantly mediated by ERα signaling, which is the main regulator of estrogen-dependent genes leading to proliferative, anabolic effects [16,17]. ERβ, when co-expressed with ERα, restrain ERα activity and its activation inhibits cell proliferation and induces a catabolic effect [16]. At high concentrations the toxicity of ZEN is independent of estrogen signaling, and exerts a cytotoxic effect characterized by a high oxidative state, cell membrane disruption, DNA oxidative damage and apoptosis [18]. ZEN has hence a pleiotropic toxicity depending on the target organ (estrogen-responding or not) and the exposure conditions (low or high dose) [19].

The intestine is exposed to food contaminants like ZEN, and is a major site of xenobiotics metabolization. In some species like human and pig, ZEN is biotransformed in the small intestine into a more estrogenic metabolite, alpha-zearalenol (α-ZOL), which explains the high sensibility of these species to this toxin [20,21]. The toxicity of ZEN in the intestine has been studied using targeted gene expression and transcriptomics both in-vitro and in-vivo, describing a regulation of the expression of genes involved in immune functions [12,14,22] as well as signaling cascades involved in the development of cancer [12,14,23]. However, more research is still needed to fully understand the

79 molecular mechanisms that lead to ZEN intestinal toxicity. Hypothesis-producing technical
80 approaches such as proteomics are particularly helpful to study toxin with multiple effects such as
81 ZEN [24], and represent a promising tool for the discovery of intestinal biomarkers of effect [19,25].
82 Nonetheless, proteomics has never been applied to investigate the toxicity of ZEN in the intestine.

83 In the present study we investigated the global proteome changes induced by a non-cytotoxic exposure
84 to ZEN using a jejunal explant model. Proteome changes indicated that ZEN mediates an estrogenic
85 activation leading to the alteration of extracellular signal-regulated protein kinases 1 and 2 (ERK1/2),
86 phosphatidylinositol 3-kinases/protein kinase B (PI3K/Akt), as well as the chemokine signaling C-X-
87 C chemokine receptor type 4/ stromal cell-derived factor 1 (CXCR4/SDF-1) axis. Functional
88 validation confirmed this hypothesis.

89

90 **2. Material and methods**

91 *2.1 Experimental Design and Statistical Rationale*

92 In the present study, an ex-vivo model based in the use of pig jejunal explants was used. This model
93 is convenient to study the molecular events dependent of the interaction between the different intestinal
94 cellular types as well as signaling gradients present along the crypt-villus axis. Additionally, it allows
95 for the analysis of control-treated paired explants, thus taking into account individual variability. The
96 pig was the chosen species because of similarities with humans regarding intestinal anatomy,
97 physiology and ZEN metabolization pattern (both species are highly sensitive due to a bioactivation
98 of ZEN through transformation to α-ZOL). Intestinal explants can be cultured ex-vivo up to 4h, and
99 longer exposure times are associated with degradative changes. Post-weaning animals are often used
100 as tissue donors because of their high sensitivity to mycotoxins [26].

To avoid unspecific molecular responses (i.e. event related with apoptosis or oxidative stress) able to mask ZEN-specific toxic events [27] we selected non-cytotoxic exposure conditions (4h at 100µM) for pig intestinal epithelial cells (Lahjouji T.; unpublished results).

Proteomic analysis and verification was performed in three paired control and treated samples (analytical sample set), whereas a second set of samples (six paired control and treated samples; validation sample set) obtained in an independent experiment under the same conditions were employed for functional analysis validation. Paired t-tests (GraphPad Software, San Diego, CA, USA) and paired ratios were employed to analyze differences in protein abundance in all cases. Significance level was set at p=0.05, and paired ratios were considered relevant if higher than 1.5.

2.2 Animals and pig jejunal explants culture

Pigs (5 weeks-old castrated males) were obtained from a local farm (Gaec de Calvignac, St. Vincent d'Autejac, France). The experiment was conducted under the guidelines of the French Ministry of Agriculture for animal research. The Ethics Committee of Pharmacology-Toxicology of Toulouse-Midi-Pyrénées approved all animal experimentation procedures in animal experimentation (Toxcométhique; N°: TOXCOM/0136/PP). Jejunal tissue collection and explants preparation was performed as detailed elsewhere [28,29] although using Williams phenol red-free (Sigma, St Quentin Fallavier, France) supplemented with 1% of insulin transferrin-selenium (Sigma), 1% penicillin (Eurobio, Courtaboeuf, France), 1% alanine-glutamine (Sigma), 0.5% gentamycin (Eurobio) and 50 mL of glucose (Sigma) as culture medium. Plates were pre-incubated for 30 min at 39°C in a humidified atmosphere with 5% CO2. Explants were exposed to ZEN (100 µM) or vehicle only (dimethylsulfoxide; DMSO; Sigma) and incubated in the same conditions for a period of 4h. After treatment, tissues were either snap frozen in liquid nitrogen and kept at -80ºC until analysis, or fixed in 10% neutral-buffered formalin. Purified ZEN was acquired from Sigma, and dissolved in DMSO to a concentration of 20 mM, aliquoted and stored at −20 °C.

2.3 Protein extraction, sodium dodecyl sulfate–polyacrylamide gel electrophoresis loading and nano-liquid chromatography–tandem mass spectrometry (nLC-MS/MS) analysis of proteins

Proteins were extracted using 2 mL plastic bead tubes (MT Biomedicals, Illkirch, France) in 0.5 mL of 6M urea, 20% SDS, 10mM Tris-HCl pH 6.8 buffer containing protease- and phosphatase inhibitors (Sigma) in a Precellys Evolution tissue homogenizer (Bertin Technologies, Montigny-le-Bretonneux, France). Total protein content was quantified (BCA protein assay, Thermo Fisher Scientific, Waltham, MA, USA). After reduction and alkylation, 100 µg of proteins were loaded on a 12% acrylamide sodium dodecyl sulfate–polyacrylamide gel and electrophoresis was performed at 50V for 20 min. Proteins were visualized as a single band by Coomassie Brilliant Blue staining. Each band was cut into a single slice that was washed in 100 mM ammonium bicarbonate for 15 min at 37°C, followed by a second wash in 100 mM ammonium bicarbonate:acetonitrile (1:1) for 15 min at 37°C. A second cycle of washes in ammonium bicarbonate and ammonium bicarbonate/acetonitrile was performed. Proteins were in-gel digested by incubating each slice with 1 µg of modified sequencing grade trypsin (Promega, Madison, WI, USA) in 50 mM ammonium bicarbonate overnight at 37°C. The resulting peptides were extracted from the gel in three steps: a first incubation in 50 mM ammonium bicarbonate for 15 min at 37°C and two incubations in 10% formic acid:acetonitrile (1:1) for 15 min at 37°C. The three collected extracts were pooled with the initial digestion supernatant, dried in a SpeedVac (Thermo Fisher Scientific), and resuspended with 50 µL of 5% acetonitrile and 0.05% trifluoroacetic acid. The peptides were analysed by nano-liquid chromatography–tandem mass spectrometry (MS/MS) using an UltiMate 3000 RSLCnano system (Dionex, Amsterdam, The Netherlands) coupled to an OrbiTrap QHF-X mass spectrometer (Thermo Fisher Scientific, Bremen, Germany). Five microliters of each sample was loaded onto a C18 pre-column (300 µm id, 5 mm; Dionex), at 20 µL/min, in 5% acetonitrile and 0.05 % trifluoroacetic acid. After 5 min of desalting, the pre-column was switched on line with the analytical C18 column (75 µm id × 15 cm C18 column; packed in-house with ReproSil-Pur C18-AQ 3 µm resin, Dr Maisch; Proxeon Biosystems, Odense, Denmark),

equilibrated in 95% solvent A (5% acetonitrile and 0.2% formic acid) and 5% solvent B (80% acetonitrile and 0.2% formic acid). Peptides were eluted using a 5–50% gradient of solvent B over 120 min and at a flow rate of 350 nL/min.

The OrbiTrap QHF-X was operated in Data Dependent Acquisition mode to automatically switch between full scan MS and MS/MS acquisition using Xcalibur software (Thermo Fisher Scientific). Survey scan MS was acquired in the Orbitrap over the m/z 350–1400 range, with the resolution set to a value of 60 000 (m/z 400). The 12 most intense ions per survey scan were selected for higher-energy collisional dissociation, and the resulting fragments were analysed in the linear ion trap. Dynamic exclusion was employed within 60s to prevent repetitive selection of the same peptide.

2.4 Bioinformatics analysis of mass spectrometry raw files and functional analysis of results

Mass spectrometry raw files were analysed using the Proline software version 1.6 [30]. MS/MS spectra were searched in the Mascot search engine (Matrix Science Inc., Boston, MA, USA) against the forward and reverse UniprotKB *Sus scrofa* database combined with a commonly observed contaminants list. The digestion enzyme was set to trypsin with up to two missed cleavages. Methionine oxidation and N-terminal acetylation were searched as variable modifications and carbamidomethyl of cysteine as fixed modification. Parent peptide masses and fragment masses were searched with maximal mass deviation of 10 ppm. A first level of false discovery rate (FDR) filtration was done on the peptide-spectrum match level, and this was followed by a second level of FDR control on the protein level. Both filtrations were performed at a 1% FDR. These filtrations were done using a standard target-decoy database approach. For label-free relative quantification of the samples, the "match between runs" option of Proline was enabled to allow cross-assignment of MS features. The mass spectrometry proteomics data have been deposited to the ProteomeXchange Consortium via the PRIDE partner repository with the dataset identifier PXD017845.

For an overview of the Gene Ontology (GO) terms regarding cellular compartment, molecular function, and biological processes in which proteins with differential abundance are involved (fold change ≥1.5 and paired t-test p-values ≤0.05), we used the DAVID Bioinformatic database v6.8 software [31]. The list of proteins showing differential abundance was also uploaded onto Ingenuity Pathway Analysis (IPA) (Qiagen Bioinformatics, Hilden, Germany) and GeneAnalytics (LifeMap Sciences, Alameda, CA; USA) software, and mapped to the respective databases of each tool. IPA uses networks, diseases, molecular and cellular functions. generated from previous publications and public protein interaction databases using the Ingenuity Knowledge Base as a reference. GeneAnalytics analysis employs and GO terms, pathways, phenotypes, and drug/compounds from GeneCards as reference. The functional analysis provided by IPA using significantly different proteins with fold change abundance ≥1.5 was not informative, so we decided to include also significantly different proteins with fold change abundance ≥1.2.

2.5 Immunoblotting analysis

Protein extracts from the analytic sample set were employed for results verification using specific antibodies for three proteins showing differential abundance, namely the thyroid hormone receptor interactor 11 (GMAP210) and Selenoprotein M (SELENOM). Functional results were validated using the validation sample set, and target proteins were estrogen receptor alpha (ERα), estrogen receptor beta (ERβ), ERK1/2, phospho-ERK1/2, nuclear factor of kappa light polypeptide gene enhancer in B-cells inhibitor alpha (IκBα), nuclear factor kappa-light-chain-enhancer of activated B cells (NF-κB), phospho-NF-κB, cyclooxygenase-2 (COX-2), caudal type homeo box transcription factor 2 protein (CDX2), Mucin-Like Protocadherin (MUCDHL), sucrose isomaltase (SI), Hypoxia Inducible Factor 1 Subunit Alpha (HIF1α), CXCR4 and SDF-1. The antibodies used for this analysis are listed in Supplemental table 1.

Proteins from jejunal explants from the validation sample set were extracted as described above, but extracted in Radioimmunoprecipitation assay (RIPA) buffer. Total protein extracts (20 µg) were

198 separated in 4-15% acrylamide-bisacrylamide gradient gels (BioRad, Hercules, CA, USA), except for
199 GMAP210, where a 10% gel was employed, and transferred onto nitrocellulose membranes. Blocking
200 was performed in RotiBlock (Carl Roth GmbH, Karlsruhe, Germany). Detection was achieved by
201 incubation with the corresponding primary antibody in blocking buffer at 4°C overnight under
202 agitation followed by the appropriate species-specific fluorescent secondary antibodies (Supplemental
203 table 1; Biotium, Inc., Fremont, CA, USA). For optimal CXCR4 detection, a treatment using Lambda
204 Protein Phosphatase was performed prior to blocking, following the manufacturer's instructions (New
205 England Biolabs Ipswich, MA, USA). Loading control consisted in total protein staining of membranes
206 using SyproRuby blot stain after blotting (Thermo Fisher Scientific). Images were obtained by
207 scanning Chemidoc (SyproRuby-stained membranes; Bio-Rad) or a Li-Cor Odyssey Infrared Imager
208 (Fluorescent immunoblots; Li-Cor Biosciences, Lincoln, NE, USA). Image Studio Lite Software (Li-
209 Cor Biosciences) was used for image analysis. Band intensity values were normalized onto the
210 respective total protein staining. Levels of phosphoproteins (phosphor- ERK1/2 and NF-κB) were
211 normalized against the corresponding non-phosphorylated protein.

212 *2.5 Histopathological and immunohistochemical analysis*

213 An histopathological evaluation was carried out, including counting of goblet cells, intraepithelial and
214 lamina propria-infiltrated immune cells. Samples from the validation sample set were fixed in 10%
215 neutral-buffered formalin, embedded in paraffin wax, sectioned at 4 µm and stained with Hematoxylin-
216 Eosin (HE; Sigma, St. Quentin Fallavier, France) for inflammatory cells and intraepithelial
217 lymphocyte counting as well as villi/crypt measurement, and Periodic Acid-Schiff (PAS; Sigma) for
218 goblet cells counting. The number of inflammatory cells in lamina propria (lymphocytes, plasma cells
219 and eosinophils), intraepithelial lymphocytes and goblet cells were counted in 10 non-overlapping and
220 consecutively selected high magnification fields of 26,000 μm^2. A photomicroscope Zeiss Axioskop
221 40 (Zeiss, Oberkochen, Germany) equipped with a digital camera Spot Insight 2 Firewire and the

222 software Spot version 4.0.5 for Windows (Spot Imaging, Diagnostics Instruments INC. Sterling
223 Heights, MI, USA) were used for the quantifications.

224 ERα immunohistochemical analysis was carried out by antigen detection using the indirect avidin–
225 biotin–peroxidase complex technique. Briefly, 4 µm tissue sections were deparaffinized and
226 rehydrated through descending graded ethanol. Endogenous peroxidase activity was quenched using
227 Dako REAL Peroxidase-Blocking Solution (Agilent, CA, USA) for 5 min at room temperature.
228 Antigen retrieval method used was pH 6 citrate buffer in a decloacking chamber for 30 min at 98ºC.
229 Sections were washed with PBS (pH 7.4) and incubated with blocking solution (normal rabbit serum,
230 dilution 1:100, Vector Laboratories, Burlingame, CA, USA) for 1 hour at room temperature in a
231 humidity chamber. ERα primary antibody diluted 1:500, was incubated overnight at 4 ºC. After
232 washing in PBS, a goat anti-rabbit IgG biotinylated polymer antibody (Vector ImmPRESS system,
233 Vector laboratories, Ca, USA) was applied for 30 min at 37ºC. Positive labeling was detected using 3,
234 3′-diaminobenzidine tetrahydrochloride (Agilent) for 5 min at room temperature. Sections were finally
235 counterstained with Mayer's hematoxylin, dehydrated and mounted. Negative controls consisting on
236 replacement of primary antibody by blocking solution were included in each assay to confirm the lack
237 of non-specific bindings. Positive cells were counted in 10 non-overlapping and consecutively selected
238 high magnification fields of 26.000 μm^2

239 **3. Results and discussion**

240 *3.1 ZEN toxicity does not involve an extensive remodeling of the jejunal proteome*

241 The clinic manifestations of mycotoxins (and other toxins) exposure result from the disruption of
242 different cell functions. These disruptions are often the consequence of the effect of that toxicant on
243 multiple molecular targets, thereby triggering a pleiotropic toxicity, whose study requires the use of
244 global technical approaches such as proteomics [24]. The mycotoxin ZEN is toxic for the intestine
245 [12,14,32], and several studies using gene expression analysis have proposed a relationship between

ZEN toxicity and immune disorders or cancer [12,14,33]. However, ZEN intestinal toxicity has not been explored yet at the proteomic level. Here, we investigated the proteome changes induced by an acute exposure to ZEN in the small intestine of male castrated pigs. Three paired jejunal explants were exposed for 4h to 100µM ZEN or vehicle (DMSO) and analyzed by nLC-MS/MS. A total of 5880 proteins were identified, of which 39 proteins were significantly over-represented, and 20 proteins were down-represented ($p \leq 0.05$ and fold change ZEN/C ≥ 1.5; Fig. 1; Table 1) in ZEN-exposed explants compared to controls. This indicates that ZEN toxicity did not involve an extensive remodeling of the proteome from intestinal cells, as only 1% of identified proteins showed significantly different abundances. This is in agreement to what is described in other proteomic studies carried out in different cell lines, where non-cytotoxic conditions were associated with a limited ZEN-dependent regulation of the proteome, between 0.15 and 3.14% of the identified proteome [6,34].

Table 1: Accession number, official gene symbol, full names and main known function of the proteins showing significant differences in pig jejunal explants exposed to 100µM of ZEN for 4h. Proteins are grouped according to the general process in which they are implicated. Paired p-values and paired ratio of treated versus control samples (N=3; ZEN/CRL) are indicated.

Accession number	Official gene symbol	Name	Paired p-value	Ratio ZEN/ CRL	Main function
Immune-related processes					
A0A0K1TQQ0_PIG	MGST2	Microsomal glutathione S-transferase 2	0.029	1.8	Leukotriene C4 production
A4ZVH1_PIG	SLA	MHC class I antigen	0.043	1.6	Antigen recognition
A0A060N3G5_PIG	SLA-3	MHC class I antigen	0.041	2.2	Antigen recognition
B1A9N3_PIG	SLA-DRB1	MHC class II antigen	0.031	0.8	Antigen recognition
A0A1C9J6B7_PIG	SLA-DRB1	MHC class II antigen	0.020	0.8	Antigen recognition
A7XP09_PIG	SLA-DRB1	MHC class II antigen	0.029	0.8	Antigen recognition
Q95311_PIG	CD74	Class II histocampatibility antigen, gamma chain	0.049	0.8	Antigen recognition
Cytoskeletal-related processes					
A0A287BA16_PIG	TRIP11	Thyroid hormone receptor interactor 11	0.046	6.3	Intracellular trafficking
A0A287AFD2_PIG	PTK2B	Protein Tyrosine Kinase 2 Beta	0.001	3.8	Reorganization of the actin cytoskeleton
B6EAV5_PIG	SLC9A3R2	Na(+)/H(+) exchange regulatory cofactor NHE-RF	0.042	3.2	Scaffold protein
I3L8H0_PIG	LOC100624559	Phosphodiesterase 4D Interacting Protein (blast) PDE4DIP	0.011	2.2	Anchoring protein
F1SAC0_PIG	FUOM	Fucose Mutarotase	0.001	2.1	Cell-cell adhesion and recognition processes
A0A286ZS05_PIG	SYNE3	Spectrin Repeat Containing Nuclear Envelope Family Member 3	0.032	2.0	Actin and actin filament binding
F1S7B0_PIG	HOOK1	Hook Microtubule Tethering Protein 1	0.019	1.8	Endocytosis mediator
AURKB_PIG	AURKB	Aurora kinase B	0.000	0.8	Involved in cytokinesis

A0A287BNG9_PIG	DBNL	Drebrin-like protein	0.018	0.6	Adapter and actin binding protein
Metabolism-related processes					
C4PK53_PIG	SELENOM	Selenoprotein M	0.045	4.6	Energy metabolism
F1RQS0_PIG	ENPP4	Ectonucleotide Pyrophosphatase/Phosphodiesterase 4	0.023	2.8	Energy metabolism
A0A287B0I6_PIG	VKORC1	Vitamin K Epoxide Reductase Complex Subunit 1	0.041	1.9	Vitamin K metabolism
F1SQH7_PIG	SLC27A2	Solute carrier family 27 (Fatty acid transporter) member 2	0.010	1.9	Lipid biosynthesis and fatty acid degradation
A0A0B8RSF3_PIG	PDPR	Pyruvate dehydrogenase phosphatase regulatory subunit	0.008	0.8	Pyruvate metabolism
F1RIS6_PIG	MMAB	Methylmalonic Aciduria (Cobalamin Deficiency) CblB Type	0.028	0.7	Vitamin B12 metabolism
Mitochondrion-related processes					
F1RWZ9_PIG	FUNDC1	FUN14 Domain Containing 1	0.006	3.1	Mitochondrial response to hypoxia
A0A0M3KL56_PIG	MRPS28	Mitoribosomal protein ms28, mrps28	0.012	1.8	Mitochondrial ribosomal proteins
F1RK50_PIG	PAM16	mitochondrial import inner membrane translocase subunit TIM16	0.046	1.8	Import of nuclear-encoded mitochondrial proteins into the mitochondrial matrix
F1SLC2_PIG	TOMM22	Translocase Of Outer Mitochondrial Membrane 22	0.019	1.6	Import cytosolic preproteins into the mitochondrion
Protein processing					
F2Z5T7_PIG	PPIL3	Peptidyl-prolyl cis-trans isomerase 3	0.016	5.1	Chaperone
GALT1_PIG	GALNT1	Polypeptide N-Acetylgalactosaminyltransferase 1	0.010	2.5	Mucin-type O-linked glycosylation
A0A287AQC9_PIG	SENP3	SUMO Specific Peptidase 3	0.014	2.4	Addition of small ubiquitin-like SUMO proteins
F1S6E6_PIG	FAF1	Fas Associated Factor 1	0.009	2.1	Ubiquitin-binding protein
A0A0B8RS63_PIG	UBXN7	UBX domain-containing protein 7	0.014	2.0	Ubiquitin-binding adapter
A0A286ZTV6_PIG	SUMF1	Sulfatase Modifying Factor 1	0.002	1.8	Catalyzes the conversion of cysteine to 3-oxoalanine
RS28_PIG	RPS28	40S ribosomal protein S28	0.021	1.7	Ribosomal protein
F1S0M9_PIG	FKBP10	FK506 Binding Protein 10	0.043	0.8	Chaperone
A0A287A8H1_PIG	UBQLN1	Ubiquilin 1	0.049	0.8	Modulation of protein degradation
F1RGQ5_PIG	UBE2G1	Ubiquitin Conjugating Enzyme E2 G1	0.025	0.8	Ubiquitin-mediated protein degradation
Transcription and RNA processing					
A0A286ZKK8_PIG	PRPF18	Pre-MRNA Processing Factor 18	0.000	4.1	RNA processing
F1RSH4_PIG	UTP18	UTP18, Small Subunit Processome Component	0.029	2.9	RNA processing
F1SCV0_PIG	ZNF511	Zinc Finger Protein 511	0.004	2.2	Transcriptional regulation
I3LPL0_PIG	WDR13	WD Repeat Domain 13	0.003	1.5	Transcriptional regulation
F1RFT0_PIG	GINS3	GINS Complex Subunit 3	0.001	0.8	Transcriptional regulation
I3L751_PIG	REXO4	REX4 Homolog, 3'-5' Exonuclease	0.041	0.8	Transcriptional regulator, can bind ESR1 and ESR2
F1RTX5_PIG	NAF1	Nuclear Assembly Factor 1 Ribonucleoprotein	0.020	0.8	RNA-binding protein
Cell signaling					
A5A8Y6_PIG	AGPAT1	1-acyl-sn-glycerol-3-phosphate acyltransferase	0.036	3.1	Lipid-related signal transduction
A0A287ANB5_PIG	BRMS1	BRMS1, Transcriptional Repressor And Anoikis Regulator	0.005	2.4	Transcriptional repressor of NF-kappa-B; anoikis promoter
A0A287A5K9_PIG	ITGA10	Integrin Subunit Alpha 10	0.003	2.3	Ahesion and cell-surface mediated signalling
A0A287B457_PIG	SMOC2	SPARC Related Modular Calcium Binding 2	0.020	1.5	Matricellular protein. Promotes matrix assembly
A0A287AZC9_PIG	FSTL1	Follistatin Like 1	0.038	0.8	Modulate the action of growth factors BMP-4 and TGF-β1 and Activin A
A0A287AAX8_PIG	CC2D1A	Coiled-coil and C2 domain containing 1A	0.015	0.8	Transcription factor
A0A286ZXA6_PIG	GADD45GIP1	GADD45G Interacting Protein 1	0.030	0.8	Cell cycle regulation. Involved in hormone response
A0A286ZWQ1_PIG	LTBP1	Latent Transforming Growth Factor Beta Binding Protein 1	0.045	0.8	Inhibit TGF-beta activity. Regulates integrin-dependent activation of TGF-beta
A0A287AIM5_PIG	CNBP	CCHC-Type Zinc Finger Nucleic Acid Binding Protein	0.019	0.8	Involved in sterol-mediated repression

Other processes					
AQP1_PIG	AQP1	Aquaporin-1	0.043	3.0	Water channel
A0A287B2D3_PIG	BRAT1	BRCA1 Associated ATM Activator 1	0.013	2.9	DNA damage response
F1RWA5_PIG	TMEM236	Transmembrane Protein 236	0.010	1.9	Unknown, highly abundant in intestinal tissues
A0A287B117_PIG	AQP11	Aquaporin 11	0.026	1.6	Water channel
F1RUH7_PIG	TPMT	Thiopurine S-Methyltransferase	0.021	0.8	Detoxification

Two highly over-represented proteins, GMAP210 and SELENOM were selected for results verification. Immunoblotting analysis confirmed the accumulation of both proteins in the jejunal explants exposed to ZEN (Fig 2), with ratios of 1.3 and 1.6, respectively. These ratios were lower than the ones obtained by proteomics (6.3 and 4.5), but the significance of the difference was higher ($p<0.01$ in both cases vs. $p<0.05$ in the case of proteomics). Differences in ratios for both techniques reflect expected differences in sensitivity, but verification is confirmed by the presence of statistical differences and the similar trend in protein accumulation.

3.2 ZEN-induced accumulation of ERα mediates an activation of NF-κB signaling without initiating an inflammatory response

The list of differentially abundant proteins (fold change ≥1.5 and paired t-test p-values ≤0.05) was analyzed using DAVID database in order to identify significantly enriched GO terms (Table 2). Overall, enriched GO terms were associated with three general three functions: (i) translational/post-translational responses, (ii) metabolic changes and (iii) NF-κB signaling.

Table 2. Enrichment of GO terms regarding cellular compartment, molecular function, and biological processes according to DAVID Bioinformatic database v6.8 functional analysis in differentially abundant proteins(fold change ≥1.5 and paired t-test p-values ≤0.05) in ZEN-treated jejunal explants.

Category GO Term Biological Process				
Reference	**Term**	**PValue**	**Fold Enrichment**	**FDR**
GO:0001961	Positive regulation of cytokine-mediated signaling pathway	0.020	95.95	0.25
GO:0006364	rRNA processing	0.024	6.28	0.29
GO:0015793	Glycerol transport	0.037	51.67	0.41

GO:0006461	Protein complex assembly	0.045	8.69	0.47
GO:0030150	Protein import into mitochondrial matrix	0.048	39.51	0.50
Category GO Term Cell Compartment				
Reference	**Term**	**PValue**	**Fold Enrichment**	**FDR**
GO:0034098	VCP-NPL4-UFD1 AAA ATPase complex	0.025	76.41	0.26
GO:0005783	Endoplasmic reticulum	0.030	2.91	0.30
GO:0031307	Integral component of mitochondrial outer membrane	0.058	32.75	0.50
Category GO Term Molecular Function				
Reference	**Term**	**PValue**	**Fold Enrichment**	**FDR**
GO:0015250	Water channel activity	0.046	41.38	0.42
GO:0016853	Isomerase activity	0.060	31.52	0.51
GO:0051059	NF-κB binding	0.085	22.07	0.64

The first function, translational/post-translational responses, was linked with the over-representation of proteins related with endoplasmic reticulum and the ATPase complex that links the endoplasmic reticulum with the proteasome system, as well as changes in rRNA processing-related proteins. Changes in the second function, cell metabolism, was indicated by the enrichment in mitochondrial proteins, isomerase activity, glycerol transport and water channel proteins. These effects can be considered unspecific cellular responses to a toxicant [27]. By contrast, the enrichment in GO terms associated with the function, NF-κB signaling (NF-κB binding and cytokine-mediated signaling), suggests a specific effect and was further investigated. NF-κB is a transcription factor mainly known for regulating the expression of numerous inducible genes involved in inflammation, but is also involved in cell differentiation, proliferation and apoptosis [35]. We observed a significant increase in the activated phosphorylated form of NF-κB, as well as in the levels of its repressor I-κBα by immunoblotting, confirming the activation of this signaling cascade (Fig.3) [35].

To determine whether this activation was associated with an inflammatory response, the abundance of COX-2, a pro-inflammatory protein targeted by NF-κB, was quantified. We did not observe any changes in the levels of this protein (Fig. 3). Using the same exposure conditions, we previously demonstrated that ZEN does not induce either the expression nor the accumulation of pro-

296 inflammatory molecules such as cytokines or acute phase proteins [32]. Our results suggest that ZEN
297 induces the activation of NF-κB cascade, but blocks the pro-inflammatory transcriptional response
298 associated with this activation. We hypothesized that the estrogenic activity of ZEN could be behind
299 this effect, since estrogen can rapidly activate and regulate NF-κB signaling [36,37], but also directly
300 control the transcriptional response of NF-κB [38].

301 We further investigated the effect of ZEN on the estrogen receptors ERβ and ERα. We observed an
302 increase in the protein levels of ERα, whereas ERβ levels remained unchanged (Fig.4). The number of
303 epithelial cells stained positive for ERα was also significantly higher in treated explants (Fig.4). ER-
304 mediated activation of NF-κB is associated with a pro- or anti-inflammatory outcome depending on
305 the preponderance of ERβ or ERα signaling, respectively [39]. The preponderance of ERα is
306 considered to be anti-inflammatory and cytoprotective [39], thus suggesting that ZEN, through its ERα
307 agonist activity, is able to induce an activation of NF-κB that is not associated with the induction of
308 inflammation.

309 *3.3 ZEN induces CXD2 and HIF1α signaling in a process that involves ERK1/2 and PI3K/Akt*
310 *activation*

311 Given that functional analysis carried out with IPA using proteins that showed significantly different
312 abundance (p-value<0.05) and fold change ≥1.5 was not informative enough, we decided to enrich the
313 functional analysis adding significantly abundant with a fold-change ≥1.2.

314 **Table 3.** Top canonical pathways enriched in differentially abundant proteins (fold change ≥1.2 and
315 paired t-test p-values ≤0.05) in ZEN-treated jejunal explants according to Ingenuity Pathway
316 Analysis.

Number	Ingenuity Top Canonical Pathways	log(p-value)	Ratio
1	CDP-diacylglycerol Biosynthesis I	2.37	0.100
2	Phosphatidylglycerol Biosynthesis II (Non-plastidic)	2.28	0.091
3	Lipid Antigen Presentation by CD1	2.14	0.077
4	Regulation of eIF4 and p70S6K Signaling	2.11	0.025
5	eNOS Signaling	2.09	0.025

317

We observed that the top enriched canonical pathways obtained by IPA (Table 3) were related with cell membrane lipids signaling, and more specifically with phosphatidylinositol 3-kinase (PI3K) signaling. Indeed, CDP-diacylglycerol (pathway 1) is involved in the regulation of lipid-dependent membrane signal transduction processes, and is an intermediate in the synthesis of phosphatidylglycerol (pathway 2) and phosphatidylinositol (PI) [40]. PI is the substrate of PI3K, a key molecule in signaling implicated in cell proliferation and metabolism [41]. PI3K, is able to activate eNOS [42,43] (pathway 4) and eIF4e (pathway 5) pathways [44]. Owing to these facts, IPA pathway analysis suggest an activation of PI3K signaling by ZEN, as the connecting event between all regulated top canonical pathways. The estrogenic activity of ZEN could explain the activation of PI3K because, together with other intracellular signaling kinase cascades such as protein kinase B (Akt) and extracellular signal-regulated kinases 1/2 (ERK1/2), estrogen signaling can rapidly activate PI3K [43,45–47]. In agreement with this hypothesis, IPA analysis predicted that ERK1/2, EGFR and the estrogen receptor beta were highly interconnected in the top scoring networks constructed with the list of differential proteins (Fig.5). Because ZEN is known to activate ERK1/2 [48] and PI3K/Akt [49] in estrogen-responding tissues, and because our results showed an accumulation of ERα, we hypothesized that ZEN, mimicking estrogen, can initiate a reciprocal membrane crosstalk between ERα and EGFR signaling pathways. The latter can rapidly activates ERK1/2 in a process known to have pro-survival and growth-promoting roles in epithelial cells [58]. To confirm this hypothesis, the activation of ERK1/2 signaling was investigated.

We were not able to see any significant differences in the relative phosphorylation of ERK1/2 in ZEN-exposed intestinal explants (Fig.6). That could be due to the rapid and transient activation of ERK by estrogen signaling [50]. We thus investigated downstream events such as the changes in the signaling of two transcription factors CDX2 and HIF1α that are targets of the two kinases PI3K and ERK. We observed a significant accumulation of CDX2 and MUCDHL (Fig.6), a protein whose expression is controlled by CDX2 [51,52], confirming that ZEN activates CDX2-related signaling. CDX2

expression is controlled by ERK1/2 dynamics [53] in intestinal cells and governs key processes in the intestinal epithelium including organization, renewal and differentiation [53–56]. MUCDHL is an atypical cadherin important for brush border formation, epithelial cell differentiation and metabolism regulation [57]. ZEN also prompted a significant increase in the protein levels of HIF1α and its target SI (which is also a target of CDX2; Fig.6) [52]. HIF1α is a transcriptional factor known for being the main regulator of the physiological response to hypoxia an the control of cellular metabolism [58,59], whose activity is controlled by ERK1/2, PI3k/Akt and NF-κB signaling in non-hypoxic conditions [60–62]. The activation of both CDX2 and HIF1α signaling by ZEN is, therefore an indirect confirmation of the alteration of ERK1/2, PI3K and NF-κB signaling in the intestine, and show that ZEN toxicity influences processes important for the regeneration of the intestinal epithelium.

3.4 ZEN activates the chemokine axis CXCR4/SDF-1 and alters the intestinal immune status

Functional analysis was completed using GeneAnalytics, and enriched pathways were ranked and scored based on degree of association with the protein set (proteins with p-value<0.05 and fold change ≥1.5). Top-scoring super-pathways are presented with matching scores in Table 5. The highest score was for the generic pathway "metabolism" followed by two specific pathways "CXCR4-mediated signaling events" and "MHC class II antigen presentation".

Table 5. SuperPaths enriched in differentially abundant proteins (fold change ≥1.5 and paired t-test p-values ≤0.05) in ZEN-treated jejunal explants according to GeneAnalytics.

GeneAnalytics SuperPaths	Score	Ratio
Metabolism	14.51	0.012
CXCR4-Mediated Signaling Events	13.75	0.066
MHC Class II antigen presentation	11.73	0.049

The involvement of CXCR4 signaling in ZEN intestinal toxicity was confirmed by immunoblotting, as CXCR4 receptor and its ligand SDF-1 were significantly up-accumulated in exposed explants (Fig.7). CXCR4 is a G-protein-coupled receptor that is activated by the chemokine stromal cell-derived

365 factor 1 (SDF-1 or CXCL12) [63]. An complete autocrine loop between ERα and CXCR4/SDF-1
366 signaling pathways is known to be installed in estrogen-depending growing cells [64,65]. ZEN-
367 induced activation of ERα response could hence promote a co-dependent accumulation of ERα,
368 CXCR4 and SDF-1. CXCR4/ SDF-1 is essential for the epithelial barrier maturation and restitution
369 through coordination with the PI3K/Akt and ERK1/2 response [63]. Hence, the disruption the CXCR4/
370 SDF-1 axis by the ZEN estrogenic effect in the intestine seems to be related with that of PI3K/Akt and
371 ERK1/2.

372 Our results indicated that ZEN can modulate the immune status of the intestine. This is suggested by
373 (i) the activation of the chemotactic axis CXCR4/ SDF-1, (ii) the increase of class I major
374 histocompatibility complex (MHC-I) proteins and a depletion of class II major histocompatibility
375 complex (MHC-II) proteins, together with (iii) the modulation of proteins linked with lipid antigen
376 presentation by CD1 (IPA canonical pathway 3 in Table 3). Epithelial cells express both MHC-I and
377 MHC-II on their surface [82]. MHC-I is expressed in all nucleated cells and are required for
378 recognition and subsequent killing of presenting cells by cytotoxic T lymphocytes, whereas MHC-II
379 is expressed by antigen-presenting cells and induces adaptive responses [82,83]. The equilibrium
380 between both systems in epithelial cells regulates the balance between intestinal tolerance and
381 inflammation [83]. Moreover, the estrogenic activity of ZEN can also explain the morphologic changes
382 observed in the intestinal tissues, namely the increased number of goblet cells and infiltrated
383 lymphocytes in the lamina propria (Fig. 8). Estrogen, as well as ZEN are known to regulate the quantity
384 of goblet cells in the intestine [66–68]. ZEN-induced increase of SDF-1 levels, a known
385 chemoattractant for T lymphocytes [81], could also explain the increase number of lymphocytes
386 infiltrating the lamina propria, a phenomenon already reported in the pig intestine upon exposure to
387 ZEN [67,68]. These results indicate that ZEN can disturb the immune status of the intestine, increasing
388 immune cells recruitment and modulating the immune sensing system.

389 **4. Conclusion**

A short, non-cytotoxic exposure to ZEN induced only few variations in the proteome of intestinal explants. Nevertheless, these changes suggested the disruption of several signaling cascades, namely ER, PI3K/Akt, NF-κB, ERK1/2 and CXCR4. These results were further validated by immunoblotting and confirmed the ablity of ZEN to activate ERα, NF-κB, PI3K/Akt, NF-κB, CDX2, HIF1α and CXCR4/SDF-1 signaling pathway. Deregulation of the dynamics of the signaling cascades mentioned above is related with the pathogenesis of several intestinal diseases, including cancer [50,69,70] and inflammatory diseases [39,63,71]. Additionally, ZEN modulated intestinal immune surveillance by increasing immune cells recruitment and shifting the innate immune sensing system. It would be advisable to investigate the effect of ZEN in the proteome of other intestinal tissues, such as duodenum and colon, as well as in animals of different sex and age. Further research is needed to investigate role of ZEN in the pathogenesis of intestinal diseases.

Funding: This project received funding from the European Union's Horizon 2020 research and innovation program under the Marie Skłodowska-Curie grant agreement No. 722634 as well as by the Agence Nationale de la Recherche (ANR) grant ExpoMycoPig (ANR-17-Carn012). The work was also supported in part by the Région Occitanie, European funds (Fonds Européens de Développement Régional, FEDER), Toulouse Métropole, and the French Ministry of Research with the Investissement d'Avenir Infrastructures Nationales en Biologie et Santé program (ProFI, Proteomics French Infrastructure project, ANR-10-INBS-08).

Acknowledgments: Authors would like to acknowledge the technical help of the members of the team "Biosynthesis and Toxicity of Mycotoxins" Philippe Pinton, Anne Marie Cossalter, Joëlle Lafitte, and Imourana Alassane-Kpembi. Chloé Terciolo is acknowledged for her scientific contribution.

Conflicts of Interest: The authors declare no conflict of interest.

References

[1] Appropriateness to set a group health-based guidance value for zearalenone and its modified forms, EFSA J. 14 (2018).

[2] H.K. Knutsen, J. Alexander, L. Barregård, M. Bignami, B. Brüschweiler, S. Ceccatelli, B. Cottrill, M. Dinovi, L. Edler, B. Grasl-Kraupp, C. Hogstrand, L. Hoogenboom, C.S. Nebbia, A. Petersen, M. Rose, A.C. Roudot, T. Schwerdtle, C. Vleminckx, G. Vollmer, H. Wallace, C. Dall'Asta, S. Dänicke, G.S. Eriksen, A. Altieri, R. Roldán-Torres, I.P. Oswald, Risks for animal health related to the presence of zearalenone and its modified forms in feed, EFSA J. 15 (2017).

[3] K. Kowalska, D.E. Habrowska-Górczyńska, A.W. Piastowska-Ciesielska, Zearalenone as an endocrine disruptor in humans, Environ. Toxicol. Pharmacol. 48 (2016) 141–149.

[4] A. Zinedine, J.M. Soriano, J.C. Moltó, J. Mañes, Review on the toxicity, occurrence, metabolism, detoxification, regulations and intake of zearalenone: An oestrogenic mycotoxin, Food Chem. Toxicol. 45 (2007) 1–18.

[5] D.E. Marin, G.C. Pistol, I. V Neagoe, L. Calin, I. Taranu, Effects of zearalenone on oxidative stress and inflammation in weanling piglets., Food Chem. Toxicol. 58 (2013) 408–15.

[6] M.C. Smith, E. Timmins-Schiffman, M. Coton, E. Coton, N. Hymery, B.L. Nunn, S. Madec, Differential impacts of individual and combined exposures of deoxynivalenol and zearalenone on the HepaRG human hepatic cell proteome, J. Proteomics. 173 (2018) 89–98.

[7] A.C. Gazzah, L. Camoin, S. Abid, C. Bouaziz, M. Ladjimi, H. Bacha, Identification of proteins related to early changes observed in Human hepatocellular carcinoma cells after treatment with the mycotoxin Zearalenone, Exp. Toxicol. Pathol. 65 (2013) 809–816.

[8] G.C. Pistol, C. Braicu, M. Motiu, M.A. Gras, D.E. Marin, M. Stancu, L. Calin, F. Israel-Roming, I. Berindan-Neagoe, I. Taranu, Zearalenone mycotoxin affects immune mediators,

437 MAPK signalling molecules, nuclear receptors and genome-wide gene expression in pig
438 spleen., PLoS One. 10 (2015) e0127503.

439 [9] G. Cai, K. Sun, T. Wang, H. Zou, J. Gu, Y. Yuan, X. Liu, Z. Liu, J. Bian, Mechanism and
440 effects of Zearalenone on mouse T lymphocytes activation in vitro, Ecotoxicol. Environ. Saf.
441 162 (2018) 208–217.

442 [10] W. Fan, Y. Lv, S. Ren, M. Shao, T. Shen, K. Huang, J. Zhou, L. Yan, S. Song, Zearalenone
443 (ZEA)-induced intestinal inflammation is mediated by the NLRP3 inflammasome.,
444 Chemosphere. 190 (2018) 272–279.

445 [11] E. Buoso, M. Galasso, M.M. Serafini, M. Ronfani, C. Lanni, E. Corsini, M. Racchi,
446 Transcriptional regulation of RACK1 and modulation of its expression: Role of steroid
447 hormones and significance in health and aging, Cell. Signal. 35 (2017) 264–271.

448 [12] C. Braicu, R. Cojocneanu-Petric, A. Jurj, D. Gulei, I. Taranu, A.M. Gras, D.E. Marin, I.
449 Berindan-Neagoe, Microarray based gene expression analysis of Sus Scrofa duodenum
450 exposed to zearalenone: significance to human health., BMC Genomics. 17 (2016) 646.

451 [13] M. Gajecka, L. Zielonka, M. Gajecki, Activity of zearalenone in the porcine intestinal tract,
452 Molecules. 22 (2017) 18.

453 [14] I. Taranu, C. Braicu, D.E. Marin, G.C. Pistol, M. Motiu, L. Balacescu, I. Beridan Neagoe, R.
454 Burlacu, Exposure to zearalenone mycotoxin alters in vitro porcine intestinal epithelial cells
455 by differential gene expression, Toxicol. Lett. 232 (2015) 310–325.

456 [15] G.G.J.M. Kuiper, J.G. Lemmen, B. Carlsson, J.C. Corton, S.H. Safe, P.T. Van Der Saag, B.
457 Van Der Burg, J.Å. Gustafsson, Interaction of estrogenic chemicals and phytoestrogens with
458 estrogen receptor β, Endocrinology. 139 (1998) 4252–4263.

459 [16] I. Paterni, C. Granchi, J.A. Katzenellenbogen, F. Minutolo, Estrogen receptors alpha (ERα)

460 and beta (ERβ): Subtype-selective ligands and clinical potential, Steroids. 90 (2014) 13–29.

461 [17] J. Fink-Gremmels, H. Malekinejad, Clinical effects and biochemical mechanisms associated
462 with exposure to the mycoestrogen zearalenone, Anim. Feed Sci. Technol. 137 (2007) 326–
463 341.

464 [18] W. Zheng, B. Wang, X. Li, T. Wang, H. Zou, J. Gu, Y. Yuan, X. Liu, J. Bai, J. Bian, Z. Liu,
465 Zearalenone promotes cell proliferation or causes cell death?, Toxins (Basel). 10 (2018) 184.

466 [19] I. Hennig-Pauka, F.-J. Koch, S. Schaumberger, B. Woechtl, J. Novak, M. Sulyok, V. Nagl,
467 Current challenges in the diagnosis of zearalenone toxicosis as illustrated by a field case of
468 hyperestrogenism in suckling piglets., Porc. Heal. Manag. 4 (2018) 18.

469 [20] T. Kuiper-Goodman, P.M. Scott, H. Watanabe, Risk assessment of the mycotoxin
470 zearalenone., Regul. Toxicol. Pharmacol. 7 (1987) 253–306.

471 [21] S.B. Binder, H.E. Schwartz-Zimmermann, E. Varga, G. Bichl, H. Michlmayr, G. Adam, F.
472 Berthiller, Metabolism of zearalenone and its major modified forms in pigs, Toxins (Basel). 9
473 (2017) 56.

474 [22] I. Taranu, A. Archir, G. Pistol, D. Marin, A.-M. Niculescu, Effect of Fusarium Mycotoxin
475 Zearalenone on Gut Epithelium, Bull. Univ. Agric. Sci. Vet. Med. Cluj-Napoca. Anim. Sci.
476 Biotechnol. 71 (2014) 2.

477 [23] H. Abassi, I. Ayed-Boussema, S. Shirley, S. Abid, H. Bacha, O. Micheau, The mycotoxin
478 zearalenone enhances cell proliferation, colony formation and promotes cell migration in the
479 human colon carcinoma cell line HCT116, Toxicol. Lett. 254 (2016) 1–7.

480 [24] L. Dellafiora, C. Dall'Asta, Forthcoming challenges in mycotoxins toxicology research for
481 safer food-a need for multi-omics approach, Toxins (Basel). 9 (2017) 18.

482 [25] L. Soler, I.P. Oswald, The importance of accounting for sex in the search of proteomic

signatures of mycotoxin exposure, J. Proteomics. 178 (2018) 114–122.

[26] M. Kolf-Clauw, J. Castellote, B. Joly, N. Bourges-Abella, I. Raymond-Letron, P. Pinton, I.P. Oswald, Development of a pig jejunal explant culture for studying the gastrointestinal toxicity of the mycotoxin deoxynivalenol: Histopathological analysis, Toxicol. Vitr. 23 (2009) 1580–1584.

[27] T. Rabilloud, P. Lescuyer, Proteomics in mechanistic toxicology: History, concepts, achievements, caveats, and potential, Proteomics. 15 (2015) 1051–1074.

[28] J. Lucioli, P. Pinton, P. Callu, J. Laffitte, F. Grosjean, M. Kolf-Clauw, I.P. Oswald, A.P.F.R.L. Bracarense, The food contaminant deoxynivalenol activates the mitogen activated protein kinases in the intestine: Interest of ex vivo models as an alternative to in vivo experiments, Toxicon. 66 (2013) 31–36.

[29] P. Pinton, F. Graziani, A. Pujol, C. Nicoletti, O. Paris, P. Ernouf, E. Di Pasquale, J. Perrier, I.P. Oswald, M. Maresca, Deoxynivalenol inhibits the expression by goblet cells of intestinal mucins through a PKR and MAP kinase dependent repression of the resistin-like molecule β., Mol. Nutr. Food Res. 59 (2015) 1076–87.

[30] D. Bouyssié, A.-M. Hesse, E. Mouton-Barbosa, M. Rompais, C. Macron, C. Carapito, A.G. de Peredo, Y. Couté, V. Dupierris, A. Burel, J.-P. Menetrey, A. Kalaitzakis, J. Poisat, A. Romdhani, O. Burlet-Schiltz, S. Cianférani, J. Garin, C. Bruley, Proline: an efficient and user-friendly software suite for large-scale proteomics, Bioinformatics. (2020) 118.

[31] D.W. Huang, B.T. Sherman, R.A. Lempicki, Systematic and integrative analysis of large gene lists using DAVID bioinformatics resources, Nat. Protoc. 4 (2009) 44–57.

[32] B. Przybylska-Gornowicz, B. Lewczuk, M. Prusik, M. Hanuszewska, M. Petrusewicz-Kosińska, M. Gajęcka, Ł. Zielonka, M. Gajęcki, The effects of deoxynivalenol and

zearalenone on the pig large intestine. A light and electron microscopy study, Toxins (Basel). 10 (2018) 148.

[33] C. Braicu, S. Selicean, R. Cojocneanu-Petric, R. Lajos, O. Balacescu, I. Taranu, D.E. Marin, M. Motiu, A. Jurj, P. Achimas-Cadariu, I. Berindan-Neagoe, Evaluation of cellular and molecular impact of zearalenone and Escherichia coli co-exposure on IPEC-1 cells using microarray technology., BMC Genomics. 17 (2016) 576.

[34] Ø.L. Busk, D. Ndossi, S. Verhaegen, L. Connolly, G. Eriksen, E. Ropstad, M. Sørlie, Relative quantification of the proteomic changes associated with the mycotoxin zearalenone in the H295R steroidogenesis model, Toxicon. 58 (2011) 533–542.

[35] Q. Zhang, M.J. Lenardo, D. Baltimore, 30 Years of NF-κB: A Blossoming of Relevance to Human Pathobiology, Cell. 168 (2017) 37–57. https://doi.org/10.1016/j.cell.2016.12.012.

[36] D. Xing, S. Oparil, H. Yu, K. Gong, W. Feng, J. Black, Y.F. Chen, S. Nozell, Estrogen modulates NFκB signaling by enhancing IκBα levels and blocking p65 binding at the promoters of inflammatory genes via estrogen receptor-β, PLoS One. 7 (2012) e36890.

[37] J.P. Stice, F.N. Mbai, L. Chen, A.A. Knowlton, Rapid activation of nuclear factor κb by 17β-estradiol and selective estrogen receptor modulators: Pathways mediating cellular protection, Shock. 38 (2012) 128–136.

[38] D. Kalaitzidis, T.D. Gilmore, Transcription factor cross-talk: The estrogen receptor and NF-κB, Trends Endocrinol. Metab. 16 (2005) 46–52. https://doi.org/10.1016/j.tem.2005.01.004.

[39] X. Nie, R. Xie, B. Tuo, Effects of Estrogen on the Gastrointestinal Tract, Dig. Dis. Sci. 63 (2018) 583–596.

[40] A.M. Heacock, B.W. Agranoff, CDP-diacylglycerol synthase from mammalian tissues, Biochim. Biophys. Acta - Lipids Lipid Metab. 1348 (1997) 166–172.

[41] D.A. Fruman, H. Chiu, B.D. Hopkins, S. Bagrodia, L.C. Cantley, R.T. Abraham, The PI3K Pathway in Human Disease, Cell. 170 (2017) 605–635.

[42] M.P. Haynes, L. Li, D. Sinha, K.S. Russell, K. Hisamoto, R. Baron, M. Collinge, W.C. Sessa, J.R. Bender, Src kinase mediates phosphatidylinositol 3-kinase/Akt-dependent rapid endothelial nitric-oxide synthase activation by estrogen, J. Biol. Chem. 278 (2003) 2118–2123.

[43] M.P. Haynes, D. Sinha, K.S. Russell, M. Collinge, D. Fulton, M. Morales-Ruiz, W.C. Sessa, J.R. Bender, Membrane estrogen receptor engagement activates endothelial nitric oxide synthase via the PI3-kinase-Akt pathway in human endothelial cells., Circ. Res. 87 (2000) 677–82.

[44] N. Siddiqui, N. Sonenberg, Signalling to eIF4E in cancer, Biochem. Soc. Trans. 43 (2015) 763–772.

[45] K. Moriarty, K.H. Kim, J.R. Bender, Estrogen Receptor-Mediated Rapid Signaling, Endocrinology. 147 (2006) 5557–5563.

[46] X. Yu, R.V.S. Rajala, J.F. McGinnis, F. Li, R.E. Anderson, X. Yan, S. Li, R. V. Elias, R.R. Knapp, X. Zhou, W. Cao, Involvement of Insulin/Phosphoinositide 3-Kinase/Akt Signal Pathway in 17β-Estradiol-mediated Neuroprotection, J. Biol. Chem. 279 (2004) 13086–13094.

[47] R.X.-D. Song, R.A. McPherson, L. Adam, Y. Bao, M. Shupnik, R. Kumar, R.J. Santen, Linkage of Rapid Estrogen Action to MAPK Activation by ERα-Shc Association and Shc Pathway Activation, Mol. Endocrinol. 16 (2002) 116–127.

[48] M. Wang, W. Wu, L. Li, J. He, S. Huang, S. Chen, J. Chen, M. Long, S. Yang, P. Li, Analysis of the miRNA Expression Profiles in the Zearalenone-Exposed TM3 Leydig Cell Line., Int. J. Mol. Sci. 20 (2019) 635.

552 [49] G.-L. Zhang, J.-L. Song, C.-L. Ji, Y.-L. Feng, J. Yu, C.M. Nyachoti, G.-S. Yang, Zearalenone
553 Exposure Enhanced the Expression of Tumorigenesis Genes in Donkey Granulosa Cells via
554 the PTEN/PI3K/AKT Signaling Pathway, Front. Genet. 9 (2018) 293.

555 [50] Y. Muta, M. Matsuda, M. Imajo, Divergent Dynamics and Functions of ERK MAP Kinase
556 Signaling in Development, Homeostasis and Cancer: Lessons from Fluorescent Bioimaging,
557 Cancers (Basel). 11 (2019) 513.

558 [51] I. Hinkel, I. Duluc, E. Martin, D. Guenot, J. Freund, I. Gross, Cdx2 controls expression of the
559 protocadherin Mucdhl, an inhibitor of growth and β-catenin activity in colon cancer cells,
560 Gastroenterology. 142 (2012) 875-885.e3.

561 [52] F. Boudreau, E.H.H.M. Rings, J. Moffett, G.P. Swain, P.G. Traber, Sucrase-isomaltase gene
562 transcription requires both Cdx and HNF-1 regulatory sites and is modulated by the in vivo
563 interaction between Cdx2 and HNF-1α proteins, Gastroenterology. 120 (2001) A103–A104.

564 [53] E. Lemieux, M.-J. Boucher, S. Mongrain, F. Boudreau, C. Asselin, N. Rivard, Constitutive
565 activation of the MEK/ERK pathway inhibits intestinal epithelial cell differentiation., Am. J.
566 Physiol. Gastrointest. Liver Physiol. 301 (2011) G719-30.

567 [54] F. Escaffit, F. Paré, R. Gauthier, N. Rivard, F. Boudreau, J.F. Beaulieu, Cdx2 modulates
568 proliferation in normal human intestinal epithelial crypt cells, Biochem. Biophys. Res.
569 Commun. 342 (2006) 66–72.

570 [55] A.K. San Roman, A. Tovaglieri, D.T. Breault, R.A. Shivdasani, Distinct processes and
571 transcriptional targets underlie CDX2 requirements in intestinal stem cells and differentiated
572 villus cells, Stem Cell Reports. 5 (2015) 673–681.

573 [56] H.B. Fan, Z.Y. Zhai, X.G. Li, C.Q. Gao, H.C. Yan, Z.S. Chen, X.Q. Wang, CDX2 stimulates
574 the proliferation of porcine intestinal epithelial cells by activating the mTORC1 and Wnt/β-

Catenin signaling pathways, Int. J. Mol. Sci. 18 (2017) 2447.

[57] A. Moufok-Sadoun, Rôle de la cadhérine atypique MUCDHL dans le système digestif et ses pathologies, n.d. https://tel.archives-ouvertes.fr/tel-02003540 (accessed February 10, 2020).

[58] E. Minet, G. Michel, D. Mottet, M. Raes, C. Michiels, Transduction pathways involved in hypoxia-inducible factor-1 phosphorylation and activation, Free Radic. Biol. Med. 31 (2001) 847–855.

[59] S.E. Corcoran, L.A.J. O'Neill, HIF1α and metabolic reprogramming in inflammation, J. Clin. Invest. 126 (2016) 3699–3707.

[60] P. Van Uden, N.S. Kenneth, S. Rocha, Regulation of hypoxia-inducible factor-1αa by NF-κB, Biochem. J. 412 (2008) 477–484.

[61] D. Mottet, G. Michel, P. Renard, N. Ninane, M. Raes, C. Michiels, ERK and calcium in activation of HIF-1, in: Ann. N. Y. Acad. Sci., New York Academy of Sciences, 2002: pp. 448–453.

[62] F. Agani, B.-H. Jiang, Oxygen-independent Regulation of HIF-1: Novel Involvement of PI3K/AKT/mTOR Pathway in Cancer, Curr. Cancer Drug Targets. 13 (2013) 245–251.

[63] N.P. Zimmerman, R.A. Vongsa, S.L. Faherty, N.H. Salzman, M.B. Dwinell, Targeted intestinal epithelial deletion of the chemokine receptor CXCR4 reveals important roles for extracellular-regulated kinase-1/2 in restitution, Lab. Investig. 91 (2011) 1040–1055.

[64] A. Boudot, G. Kerdivel, D. Habauzit, J. Eeckhoute, F. Le Dily, G. Flouriot, M. Samson, F. Pakdel, Differential estrogen-regulation of CXCL12 chemokine receptors, CXCR4 and CXCR7, contributes to the growth effect of estrogens in breast cancer cells, PLoS One. 6 (2011) e20898.

[65] K. Sauvé, J. Lepage, M. Sanchez, N. Heveker, A. Tremblay, Positive feedback activation of

estrogen receptors by the CXCL12-CXCR4 pathway, Cancer Res. 69 (2009) 5793–5800.

[66] N.L. Cho, S.H. Javid, A.M. Carothers, M. Redston, M.M. Bertagnolli, Estrogen receptors alpha and beta are inhibitory modifiers of Apc-dependent tumorigenesis in the proximal colon of Min/+ mice., Cancer Res. 67 (2007) 2366–72.

[67] B. Lewczuk, B. Przybylska-Gornowicz, M. Gajecka, K. Targońska, N. Ziółkowska, M. Prusik, M. Gajecki, Histological structure of duodenum in gilts receiving low doses of zearalenone and deoxynivalenol in feed, Exp. Toxicol. Pathol. 68 (2016) 157–166.

[68] K. Obremski, M. Gajecka, L. Zielonka, E. Jakimiuk, M. Gajecki, Morphology and ultrastructure of small intestine mucosa in gilts with zearalenone mycotoxicosis., Pol. J. Vet. Sci. 8 (2005) 301–7.

[69] X. Yu, D. Wang, X. Wang, S. Sun, Y. Zhang, S. Wang, R. Miao, X. Xu, X. Qu, CXCL12/CXCR4 promotes inflammation-driven colorectal cancer progression through activation of RhoA signaling by sponging miR-133a-3p, J. Exp. Clin. Cancer Res. 38 (2019).

[70] R.M. Hasson, A. Briggs, A.M. Carothers, J.S. Davids, J. Wang, S.H. Javid, N.L. Cho, M.M. Bertagnolli, Estrogen receptor α or β loss in the colon of Min/+ mice promotes crypt expansion and impairs TGFβ and HNF3β signaling., Carcinogenesis. 35 (2014) 96–102.

[71] L. Werner, H. Guzner-Gur, I. Dotan, Involvement of CXCR4/CXCR7/CXCL12 interactions in inflammatory bowel disease, Theranostics. 3 (2013) 40–46.

Figure legends

Figure 1: Volcano plot of log significance (paired t-tests) versus log paired ratio on the y and x axes of ZEN-induced changes (100μM, 4h exposure) in protein abundance. Circles represent identified proteins not showing significant differences whereas full grey dots represent proteins with significantly differences abundances between treated and control explants ($p<0.05$; ratio=1.5): Asterisks indicate two proteins, thyroid hormone receptor interactor 11 (GMAP210) and Selenoprotein M (SELENOM), showing significantly different abundance that were verified by immunoblotting.

Figure 2. Immunoblotting analysis of thyroid hormone receptor interactor 11 (GMAP210) and Selenoprotein M (SELENOM) in the analytic sample set. (A) Blot images of GMAP210 and

SELENOM in paired pig jejunal explants (1-3) exposed (Z) or not (C) to 100 µM ZEN (Z). (B) Relative quantification of normalized signal (arbitrary units). Values are means with standard errors of the mean represented by vertical bars (n = 3). Asterisks indicate statistical differences (**p < 0.01).

Figure 3. Immunoblotting analysis of phospho-NF-κB , IκBα, COX-2 in paired pig jejunal explants exposed (Z/ZEN) or not (C/CRL) to 100 µM ZEN (Z) in the validation sample set. (A) Representative blots of 3 paired samples of phospho-NF-κB, NF-κB, IκBα and COX-2 (B) Relative quantification of normalized signal (arbitrary units). Values of phospho-NF-κB were relative to those of NF-κB. Values are means with standard errors of the mean represented by vertical bars (n=6). Asterisks indicate statistical differences (*p < 0.05; **p < 0.01, ***p < 0.001).

Figure 4. Immunoblotting and immunohistochemical analysis of ERα and ERβ in paired pig jejunal explants exposed or not to 100 µM ZEN (Z) in the validation sample set. (A) Representative image of positive immunostatining in a control sample and (B) treated sample from the same animal. Examples of positive nuclear staining is indicated by arrows. (C) Quantification of positive immunostained cells in paired control (CRL) and treated (ZEN) samples (n=6) (D) Representative blots of 3 paired samples of ERα and ERβ in control (C) and treated (Z) samples and relative quantification of normalized signal (arbitrary units). Values are means with standard errors of the mean represented by vertical bars (n=6). Asterisks indicate statistical differences (*p < 0.05; **p < 0.01, ***p < 0.001).

Figure 5. Graphical representation of the molecular relationships between molecules centered around the estrogen receptor beta (ERβ), extracellular signal-regulated kinases 1/2 (ERK1/2) and epithelial growth factor receptor (EGFR) as a result of ZEN exposure to jejunal explants. Genes are represented by nodes with their shape representing the type of molecule/functional class, and the relationship between the nodes are indicated by edges. Nodes and arrows in pink represent proteins/interactions upregulated in ZEN-treated explants. White nodes are proteins not included in input set of proteins but having a strong connection to the proteins in the input list. The legend explaining node shape and edge type is given in the figure.

Figure 6. Immunoblotting analysis of paired pig jejunal explants exposed (Z) or not (C) to 100 µM ZEN (Z) in the validation sample set. (A) Representative blots of 3 paired samples of phospho-ERK1/2, ERK1/2, CDX2, MUCDHL, HIF1α and SI. (B) and (C) Relative quantification of normalized signal (arbitrary units). Values of phospho-ERK1/2 were relative to those of ERK1/2. Values are means with standard errors of the mean represented by vertical bars (n=6). Asterisks indicate statistical differences (*p < 0.05; **p < 0.01, ***p < 0.001).

Figure 7. Immunoblotting analysis of paired pig jejunal explants exposed (Z) or not (C) to 100 µM ZEN (Z) in the validation sample set. (A) Representative blots of 3 paired samples of phospho-CXCR4 and SDF-1. (B) and (C) Relative quantification of normalized signal (arbitrary units). Values are means with standard errors of the mean represented by vertical bars (n=6). Asterisks indicate statistical differences (*p < 0.05; **p < 0.01, ***p < 0.001).

Figure 8. Histopathological analysis of paired pig jejunal explants exposed (ZEN) or not (CRL) to 100 µM ZEN (Z) in the validation sample set. The table above includes the means, standard deviations of the mean and standard errors of the mean of each measure are indicated, along with the level of the statistical differences (n=6). For more details on how measures were obtained, the reader is referred to the material and methods section 2.5. (A) Aspects of normal numbers of lamina propria infiltrated lymphocytes in a control sample and (B) increased lamina propria lymphocytes infiltration in the paired treated sample.HE; bar 20 µm. (C) Aspect of normal numbers of goblet cells in in a control sample stained and (D) increased number of goblet cells. PAS; bar 20 µm. Arrows indicate examples of each measure in the image.

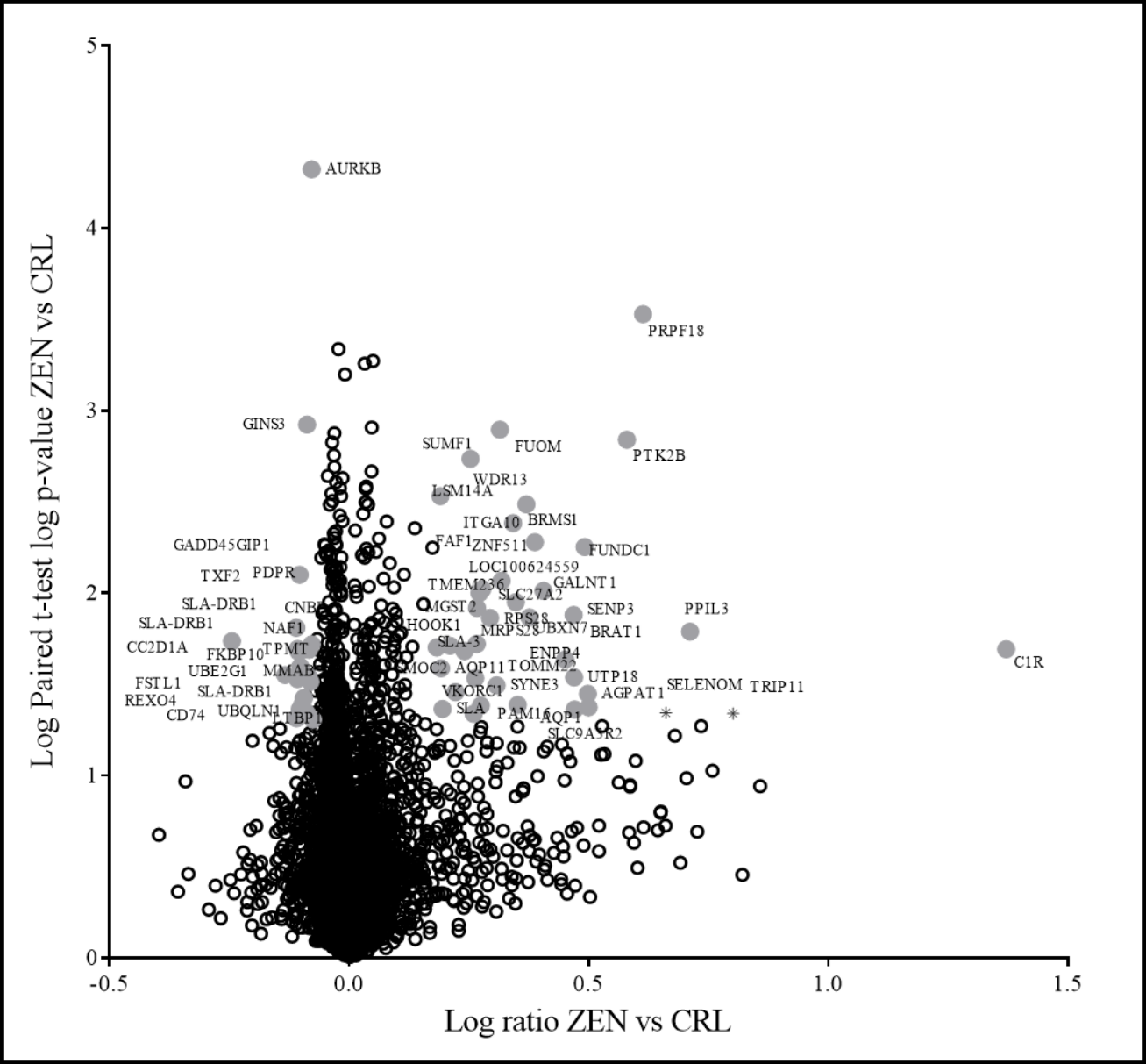
Log Paired t-test log p-value ZEN vs CRL
Log ratio ZEN vs CRL
5
4
3
2
1
0
-0.5
0.0
0.5
1.0
1.5
AURKB
PRPF18
GINS3
SUMF1
FUOM
PTK2B
WDR13
LSM14A
ITGA10
BRMS1
GADD45GIP1
FAF1
ZNF511
FUNDC1
LOC100624559
TXF2
PDPR
TMEM236
GALNT1
SLC27A2
SLA-DRB1
CNB
MGST2
SENP3
PPIL3
SLA-DRB1
NAF1
HOOK1
RPS28
MRPS28
UBXN7
BRAT1
CC2D1A
FKBP10
TPMT
SLA-3
ENPP4
C1R
UBE2G1
MMAB
SMOC2
AQP11
TOMM22
UTP18
FSTL1
SLA-DRB1
VKORC1
SYNE3
AGPAT1
SELENOM
TRIP11
REXO4
CD74
UBQLN1
LTBP1
SLA
PAM16
AQP1
SLC9A3R2

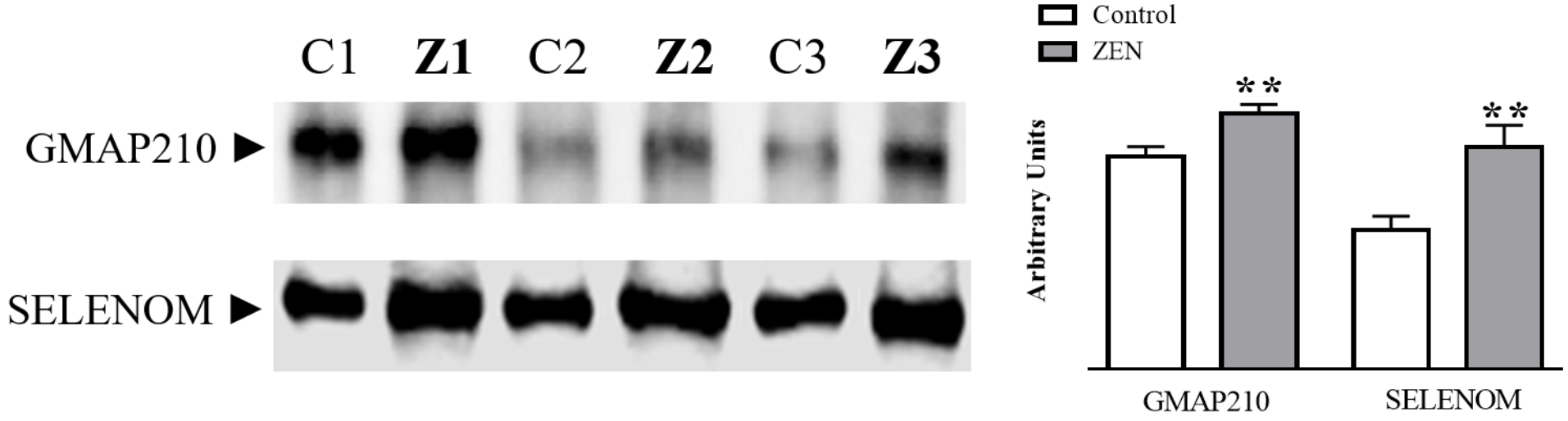
C1
Z1
C2
Z2
C3
Z3
GMAP210 ►
SELENOM ►
Control
ZEN
Arbitrary Units
**
**
GMAP210
SELENOM

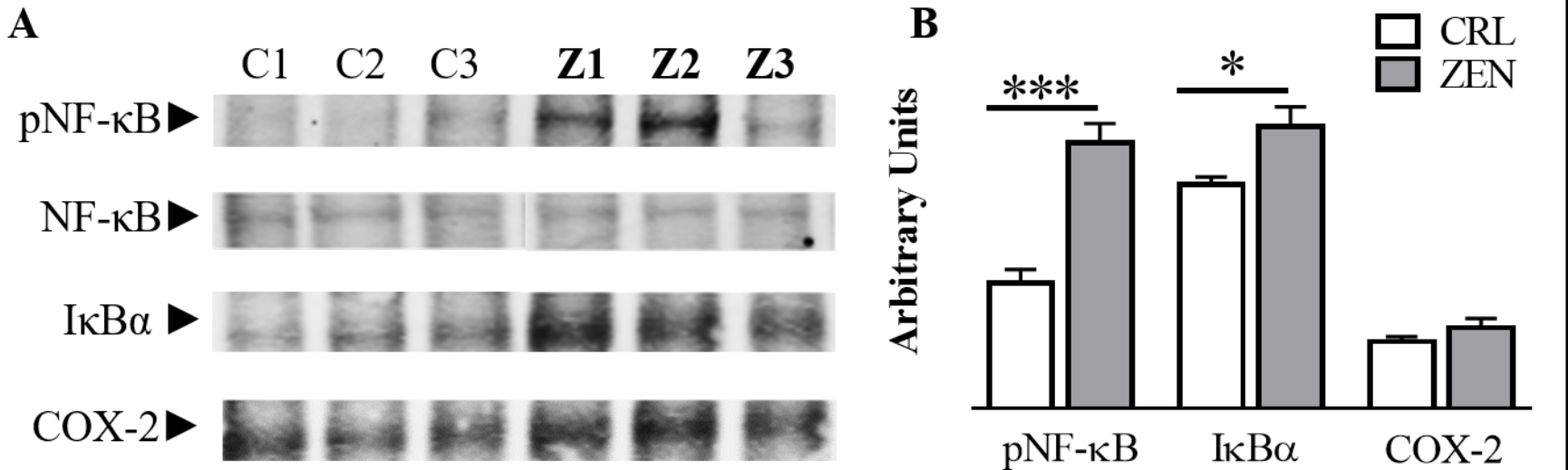
A
C1
C2
C3
Z1
Z2
Z3
pNF-κB▶
NF-κB▶
IκBα ▶
COX-2▶
B
Arbitrary Units
***
*
CRL
ZEN
pNF-κB
IκBα
COX-2

A

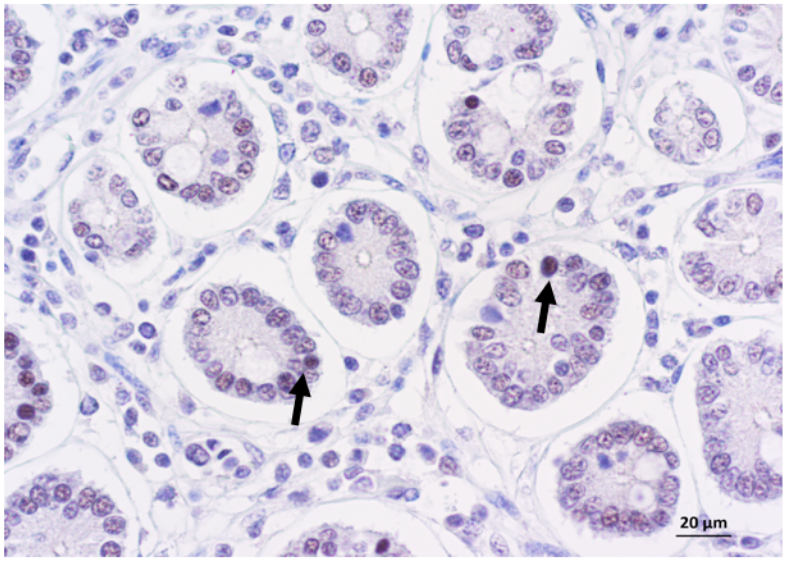
20 µm

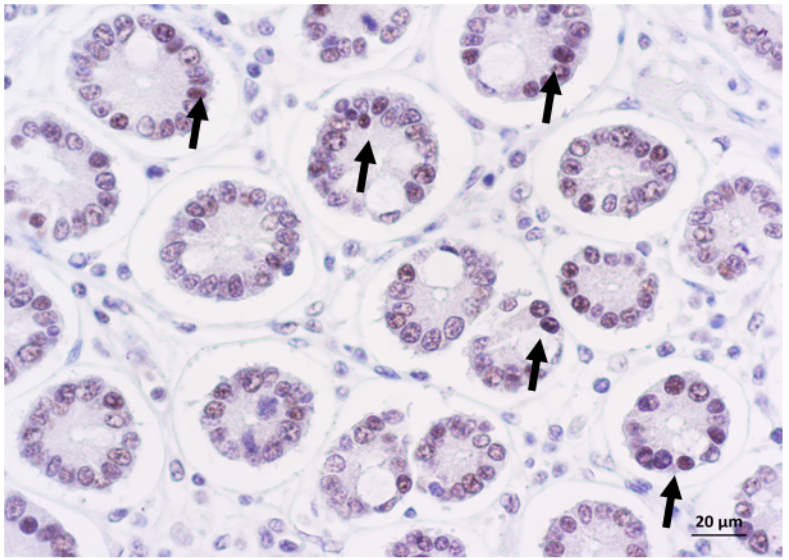
20 µm

B

C

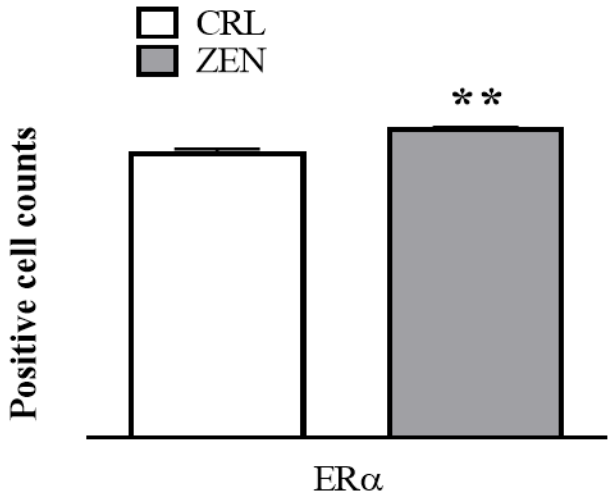
CRL
ZEN
**
Positive cell counts
ERα

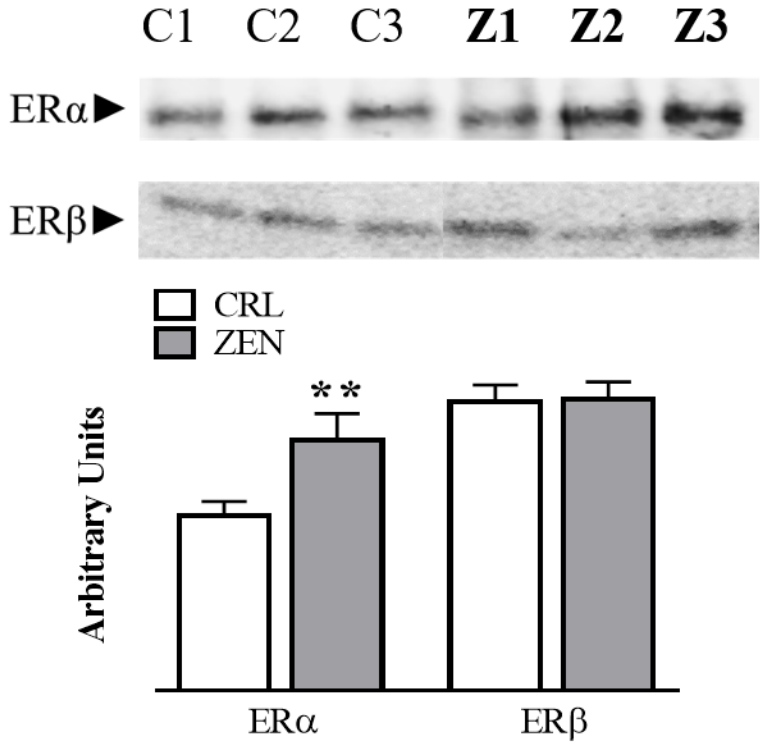
C1
C2
C3
Z1
Z2
Z3
ERα▶
ERβ▶
CRL
ZEN
**
Arbitrary Units
ERα
ERβ

D

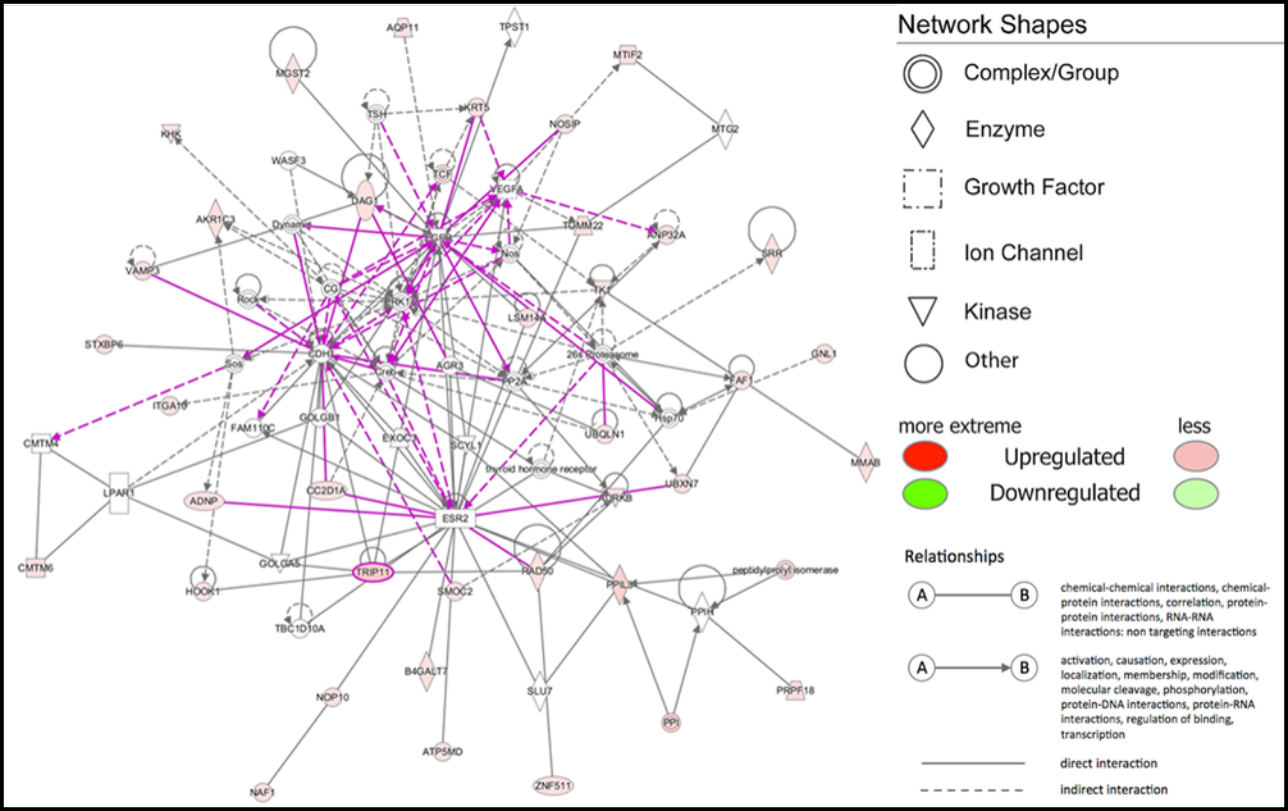

Network Shapes

- Complex/Group
- Enzyme
- Growth Factor
- Ion Channel
- Kinase
- Other

more extreme — less

- Upregulated
- Downregulated

Relationships

- A — B: chemical-chemical interactions, chemical-protein interactions, correlation, protein-protein interactions, RNA-RNA interactions: non targeting interactions
- A → B: activation, causation, expression, localization, membership, modification, molecular cleavage, phosphorylation, protein-DNA interactions, protein-RNA interactions, regulation of binding, transcription
- direct interaction
- indirect interaction

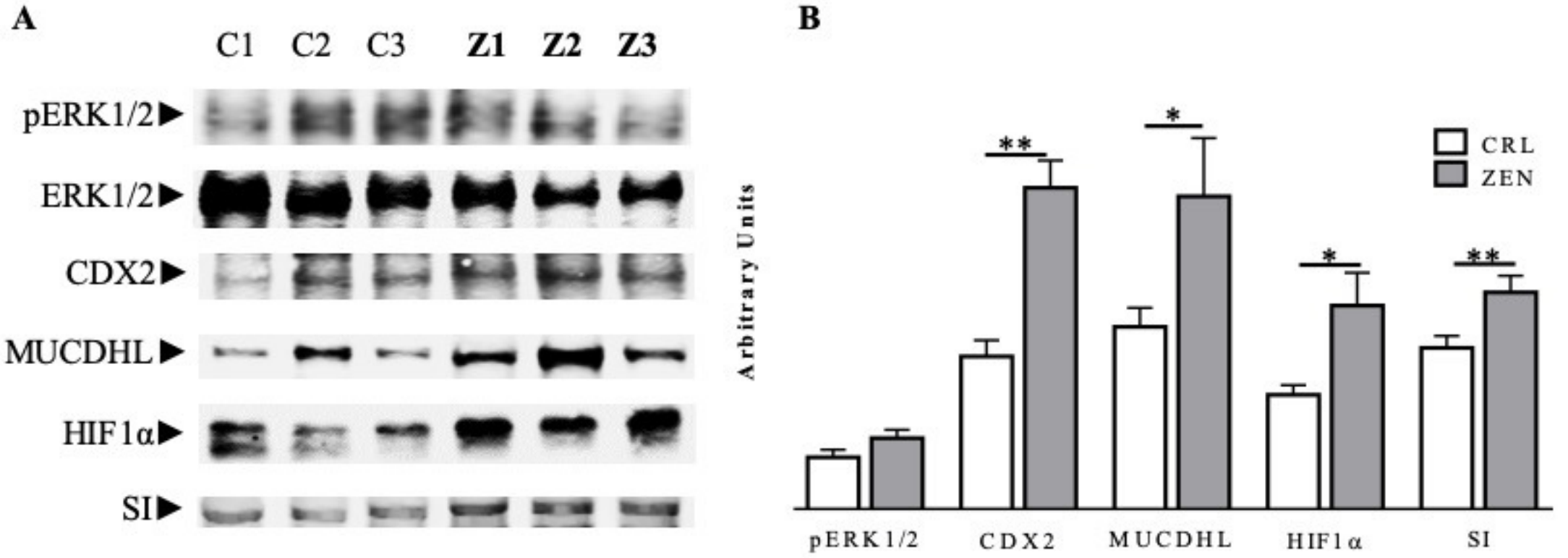
A
C1
C2
C3
Z1
Z2
Z3
pERK1/2
ERK1/2
CDX2
MUCDHL
HIF1α
SI
B
Arbitrary Units
CRL
ZEN
**
*
*
**
pERK1/2
CDX2
MUCDHL
HIF1α
SI

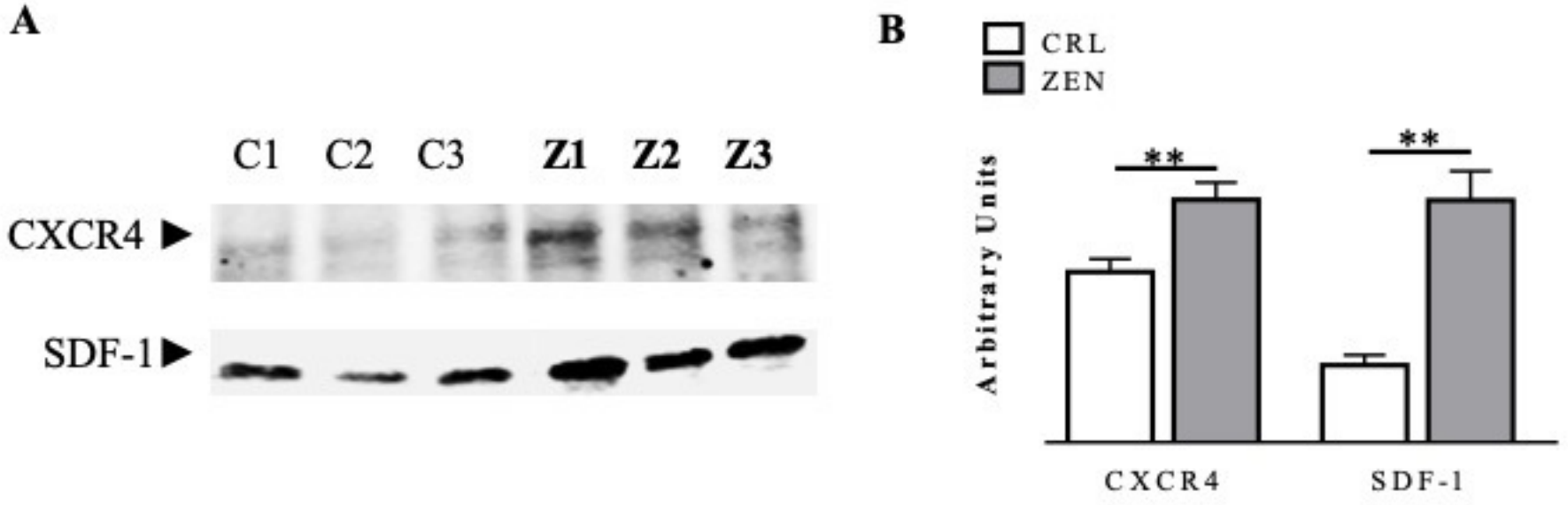
A
C1
C2
C3
Z1
Z2
Z3
CXCR4 ▶
SDF-1 ▶
B
CRL
ZEN
Arbitrary Units
**
**
CXCR4
SDF-1

Parameter	Intrepithelial lympocytes		Goblet cells		Plasmatic cells		Lamina propria lympocytes		Eosinophils	
	CRL	ZEN	CRL	ZEN	CRL	ZEN	CRL	ZEN	CRL	ZEN
Mean	1.8	2.06	13.03	14.4	3.2	3.1	6.3	7.7	4.7	6
SD	1.03	1.05	3.2	2.6	1.2	1.3	2.3	3.4	2.7	3.8
SEM	0.1	0.1	0.4	0.3	0.1	0.1	0.3	0.4	0.3	0.5
Significance level	n.s.		p<0.01		n.s.		p<0.05		n.s.	

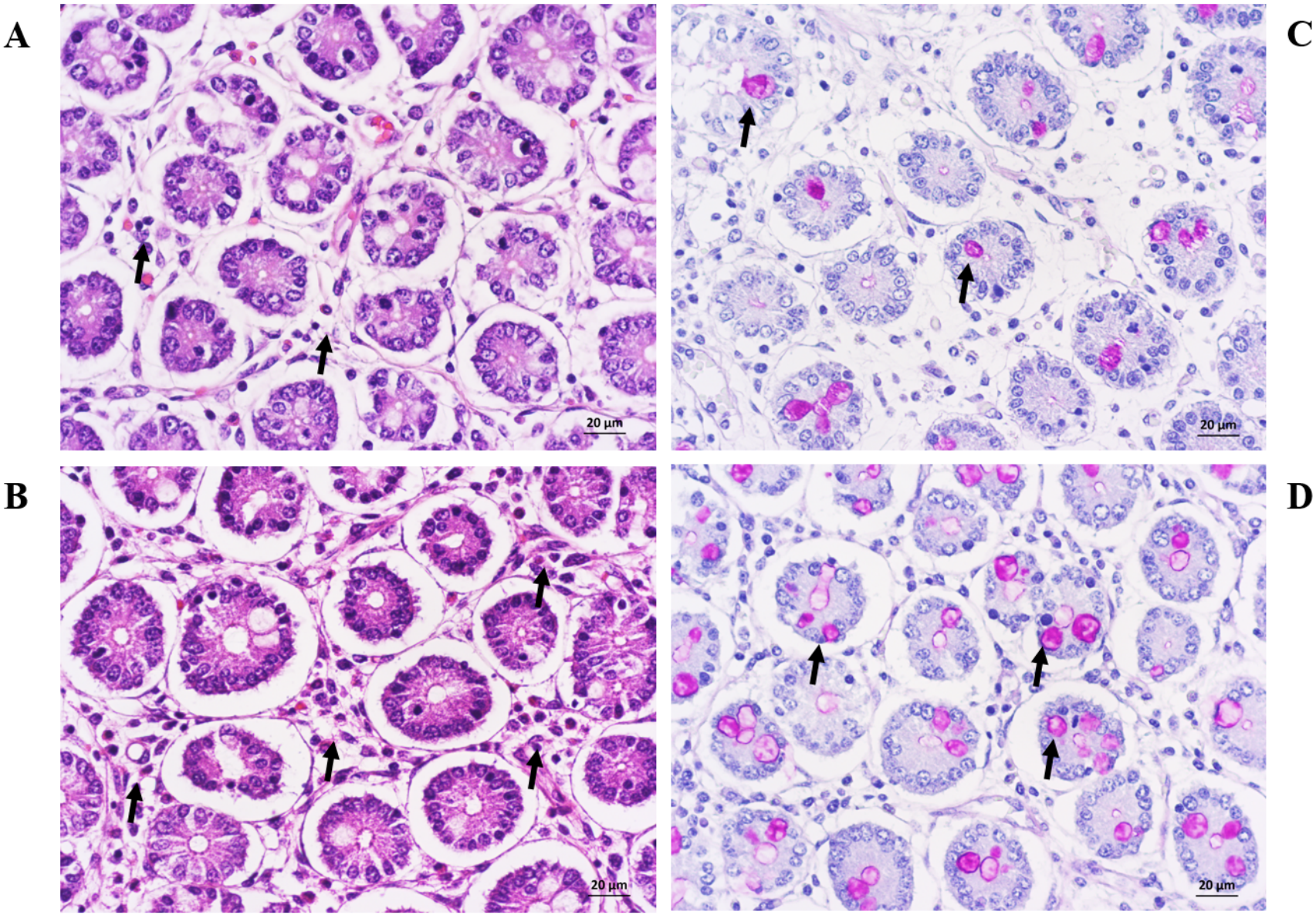

Mechanism of toxicity of the mycotoxin Zearalenone (ZEN) in the pig small intestine as revealed by proteomic analysis